CrystEngComm

PAPER

View Article Online
View Journal | View Issue

Check for updates

Cite this: *CrystEngComm*, 2024, **26**, 4871

Light-up covalent organic frameworks with flexible wall design for chemical sensing†

Wanyi Zhao,[a] Ce Xing,[a] Yuwei Zhang, *[a] Juntao Ren*[b] and He Li *[b]

Received 24th June 2024,
Accepted 4th August 2024

DOI: 10.1039/d4ce00635f

rsc.li/crystengcomm

Covalent organic frameworks (COFs) are a novel type of nanoporous and crystalline polymers with a precise and highly conjugated skeleton, making them promising candidates for constructing emissive materials. However, the strong high conjugation structures between adjacent layers easily lead to aggregation-caused quenching (ACQ) of emission properties. In this study, we have designed COFs with a flexible skeleton to suppress ACQ effects, enhancing their luminescence activity. In addition, the high density of nitrogen and oxygen atoms on these flexible walls serves as binding sites for hydrogen bonding interactions, indicating sensitivity and selectivity towards nitro-explosives. This strategy establishes a new approach for creating luminescent materials for chemical sensors.

Open Access Article. Published on 08 August 2024. Downloaded on 2/7/2026 4:39:54 PM.
This article is licensed under a Creative Commons Attribution-NonCommercial 3.0 Unported Licence.

Introduction

Covalent organic frameworks (COFs) represent a novel class of porous organic materials characterized by excellent crystallinity and porosity.[1–5] Generally, COFs are composed of light elements such as carbon, hydrogen, oxygen, and nitrogen, connected by organic bonds through reversible reactions, which indicate their remarkable stability.[6–8] The synthesis strategy is based on the geometric topology, yielding a highly ordered structure.[9–15] Benefiting from the versatility of organic reactions and the availability of various topologies, different structures can be generated, leading to a wide range of applications, including gas adsorption, catalysis, energy storage, and luminescence sensing.[16–41]

Recently, many researchers have shown a deep interest in emissive materials due to their practical applications, such as hazardous substance detection, bioimaging, illumination, and many more.[7–9] COFs maintained precise and highly conjugated skeletons, making them promising candidates for designing and producing emissive materials. However, the strong high-conjugate structures between adjacent layers can easily lead to aggregation-caused quenching (ACQ) of emissive properties.[18–25] With these considerations in mind, various approaches have been employed to enhance the luminescence of COFs. Using fluorescent monomer construction materials seems to be a very simple and effective way. However, in most cases, this strategy has little to no effect, resulting in either no fluorescence or very weak fluorescence.[7–9] More recently, Banerjee *et al.* achieved uniform nanosheets through a simple mechanical peeling method, resulting in a fluorescent chemosensor.[27] Liu *et al.* designed a monomer with *tert*-butyl units to synthesize highly emissive COFs for a copper sensor with good selectivity and sensitivity.[28] Another effective approach involves introducing long alkyl chains into COF channels, resulting in emissive COFs.[29,30] Furthermore, utilizing multi-component building units with different alkyl chains have led to broad emission spectra, with some emission close to near-white light.[31] Recently, flexible linkers have been incorporated into the COF structure, significantly influencing the luminescence properties of COFs.[32] Although substantial progress has been made in all of the aforementioned areas, exploration of light-emitting COFs is also a worthwhile endeavour.

In this study, we designed flexible walls to light up COFs, significantly improving their emissive properties. The flexible unit, denoted as 4,4′,4″-((1,3,5-triazine-2,4,6-triyl)tris(oxy)) trianiline (TTTTA), serves as the vertex, while other units, such as 3-hydroxy-[1,1′-biphenyl]-4,4′-dicarbaldehyde (BP-OH-1) and 3,3′-dihydroxy-[1,1′-biphenyl]-4,4′-dicarbaldehyde (BP-OH-2), act as linkers. These components are used to construct TTTT-COF-1 and TTTT-COF-2 as illustrated in Fig. 1. In this design, the flexible channels effectively mitigate aggregation effects caused by strong conjugation between layers, leading to enhanced luminescence. Furthermore, the presence of hydroxyl groups and nitrogen atoms in the linkage results in hydrogen-bonding interactions, referred to as excited-state intramolecular proton transfer (ESIPT).[33]

[a] *Laboratory of Preparation and Applications of Environmental Friendly Materials (Jilin Normal University), Ministry of Education, Changchun, 130103, China. E-mail: yw_zhang@jlnu.edu.cn*
[b] *Division of Energy Materials, Dalian Institute of Chemical Physics, Chinese Academy of Sciences, Dalian 116023, China. E-mail: jtren@dicp.ac.cn, lihe@dicp.ac.cn*

† Electronic supplementary information (ESI) available. See DOI: https://doi.org/10.1039/d4ce00635f

Open Access Article. Published on 08 August 2024. Downloaded on 2/7/2026 4:39:54 PM.
This article is licensed under a Creative Commons Attribution-NonCommercial 3.0 Unported Licence.

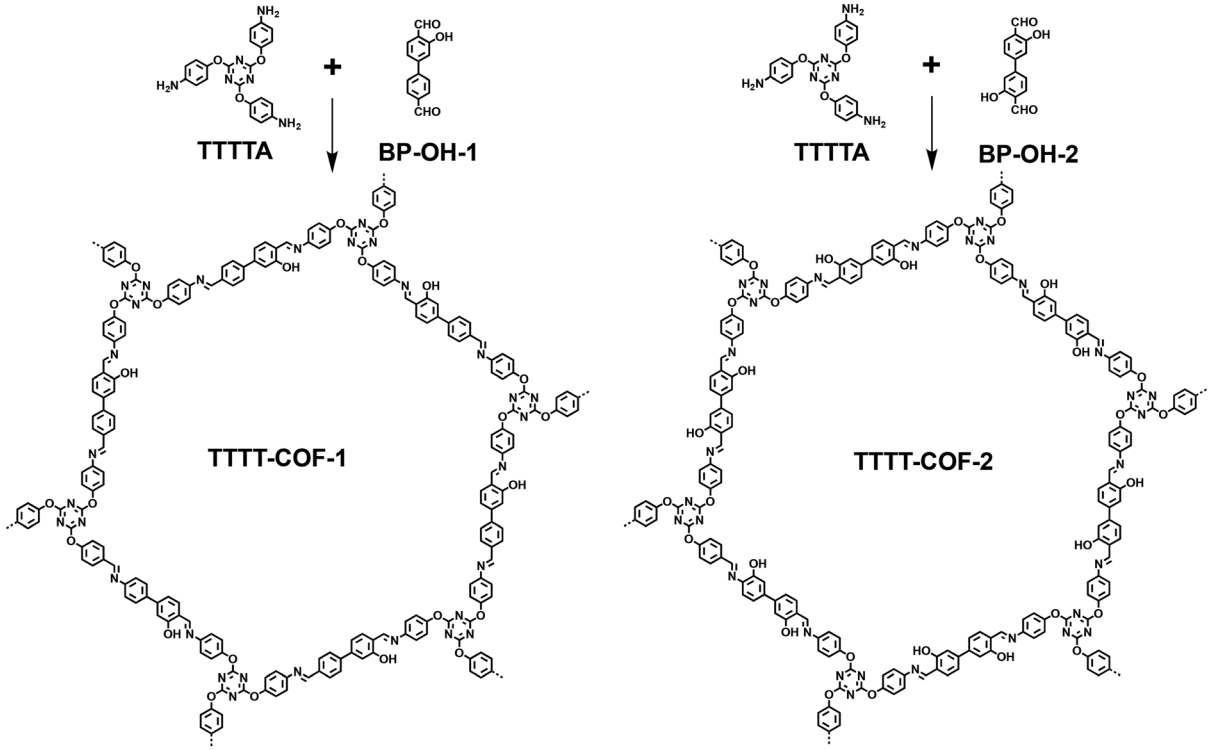

Fig. 1 Schematic illustration for the synthesis of TTTT-COF-1 and TTTT-COF-2.

These features contribute to the outstanding emission capability of the COFs. Notably, the high-density nitrogen and oxygen atoms within the flexible channels serve as sites for hydrogen-bonding interactions with nitro-explosives. This imparts remarkable sensitivity and selectivity towards nitro-explosives in TTTT-COFs, surpassing the capabilities of reported detectors.

Results and discussion

TTTT-COF-1 and TTTT-COF-2, both featuring flexible channels, were obtained through a Schiff base reaction followed by a simple purification process. To characterize their chemical structures, Fourier transform infrared spectroscopy (FT-IR) analysis revealed imine linkage vibrations at 1595 and 1596 cm^{-1} for TTTT-COF-1 and TTTT-COF-2, respectively (Fig. S1†). The triazine centers were observed at 1569 and 1571 cm^{-1} for TTTT-COF-1 and TTTT-COF-2, respectively. The solid ^{13}C nuclear magnetic resonance (NMR) spectra of TTTT-COF-1 and TTTT-COF-2 exhibited the carbon of the imine linkage at 162 ppm and the triazine center at 174 ppm (Fig. S2†). The carbons of aryl units for both COFs were located from 110 to 150 ppm. Field emission scanning electron microscopy (FE-SEM) revealed a uniform stacking morphology (Fig. S3†). The energy dispersive spectroscopy (EDS) mapping of the two TTTT-COFs showed a uniform distribution of carbon, nitrogen and oxygen elements (Fig. S4 and S5†).

The permanent porosities of TTTT-COFs were assessed through nitrogen sorption experiments conducted at 77 K. The nitrogen adsorption curves for TTTT-COF-1 and TTTT-COF-2 revealed a type-IV sorption isotherm, indicative of their mesoporous nature (Fig. S6a and S7a†). The Brunauer–Emmett–Teller (BET) surface areas were calculated to be 560 $m^2\ g^{-1}$ for TTTT-COF-1 and 175 $m^2\ g^{-1}$ for TTTT-COF-2, respectively. The primary pore size was predominantly centered at about 3.7 nm for both TTTT-COFs (Fig. S6b and S7b†). Mesopores could facilitate the diffusion and transport of adsorbates within the pore channels.

The crystalline nature of TTTT-COFs was confirmed through powder X-ray diffraction (PXRD) analysis. TTTT-COF-1 exhibited a strong peak at 2.16° and relatively weaker peaks at 3.82°, 5.94°, 7.84°, and 9.76° (Fig. 2a, red), corresponding to the (110), (200), (210), (220), and (220) facets, respectively. Similar results were observed for TTTT-COF-2, with distinct signals at 2.20°, 3.96°, 6.08°, 8.12°, and 10.16° (Fig. 2c, red), corresponding to the (110), (200), (210), (220), and (220) facets, respectively. After the Pawley refinement of unit cells, the AA stacking model for TTTT-COFs closely matched the observed patterns, while the AB model was not suitable. The unit cells of the AA model of both COFs are illustrated in Fig. 2b and d. The optimized simulation parameters for TTTT-COF-1 were $\alpha = \beta = 90°$, $\gamma = 120°$, $a = b = 46.5468$ Å, and $c = 3.5068$ Å (R_{wp}: 5.10% and R_p: 3.85%). For TTTT-COF-2, the optimized simulation parameters were $\alpha = \beta = 90°$, $\gamma = 120°$, $a = b = 46.5355$ Å, and $c = 3.5045$ Å (R_{wp}: 5.59% and R_p: 3.64%). PXRD analysis

 This journal is © The Royal Society of Chemistry 2024

Open Access Article. Published on 08 August 2024. Downloaded on 2/7/2026 4:39:54 PM.
This article is licensed under a Creative Commons Attribution-NonCommercial 3.0 Unported Licence.

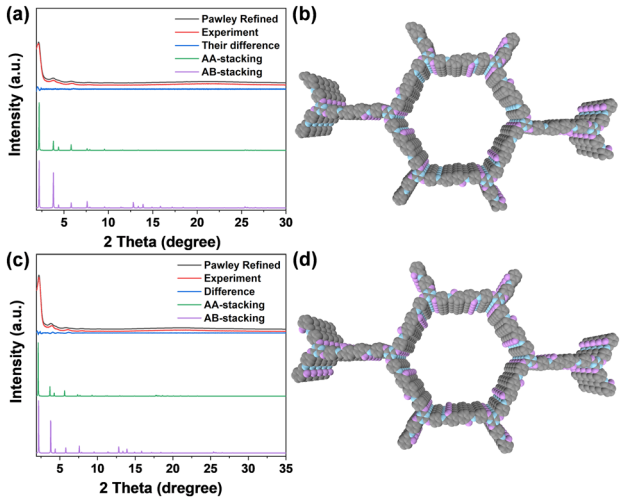

Fig. 2 Experimental, Pawley-refined, simulated PXRD patterns and the difference plots of the PXRD patterns of (a) TTTT-COF-1 and (c) TTTT-COF-2. Unit cells of (b) TTTT-COF-1 and (d) TTTT-COF-2.

demonstrated that TTTT-COFs form a highly crystalline network.

Comparing these constructed monomers, TTTT-COFs exhibited high conjugation, as evidenced by their red-shifts in the solid absorption spectra (Fig. 3a and b). The emission properties of the TTTT-COF powder were initially assessed using fluorescence spectra. Both powders emitted yellow fluorescence with emission peaks at 548 nm (TTTT-COF-1, Fig. 3c) and 561 nm (TTTT-COF-2, Fig. 3d). The absolute fluorescence quantum yields were determined to be 12.3% and 17.63% using the integrating sphere method.

Explosives are known to pose a significant threat to the environment, as their release can lead to the contamination of soil and aquatic ecosystems.[34,42] Nitroaromatic compounds, such as 2,4,6-trinitrophenol (TNP), 2,4-dinitrophenol (DNP), 2-nitrophenol (NP), 2,4-dinitrotoluene (DNT), 2-nitrotoluene (NT), and nitrobenzene (NB) serve as typical examples. The TTTT-COF samples exhibit excellent porosity, a mesoporous structure, and flexible channels, which provide ample space for capturing guest molecules through pore functionality. Furthermore, their strong emission capabilities suggest lower detection limits for molecule detectors. The high-density nitrogen and oxygen atoms within the flexible channels serve as hydrogen bond acceptors for nitroaromatic compounds.[33,35,36] The TTTT-COF samples were simply treated with ultrasound to achieve uniform dispersion in tetrahydrofuran. Interestingly, TTTT-COF-1 exhibited a significant emission quenching response towards TNP with high efficiency at 65% (Fig. 4a and b), while the addition of other nitroaromatic compounds had little impact on their emissions (Fig. S8a–S12a†). Similarly, TTTT-COF-2 displayed good selectivity and efficiency with a 76% quenching response towards TNP (Fig. 4c and d). The high quenching efficiency is due to the blockage of the ESIPT process by hydroxyl groups and nitrogen atoms. In the presence of nitroaromatic compounds, the nitrogen and oxygen atoms serve as hydrogen bond acceptors, effectively preventing the ESIPT process and leading to significant fluorescence quenching.[23,33,35] The relative lower quenching efficiencies of TTTT-COF-2 towards other compounds were obtained at 19%, 13%, 7%, 5%, and 5% for DNP, DNT, NP, NT, and NB, respectively (Fig. S8b–S12b†).

The detection limit is a crucial parameter for chemical sensors. As the concentration of TNP increased, the fluorescence intensity of both TTTT-COFs gradually decreased (Fig. 4b and d). The emission intensity and TNP concentration exhibited an almost proportional relationship at lower concentrations, resulting in a detection limit of 148 nM for TTTT-COF-1 (Fig. S13a†) and 83 nM for TTTT-COF-2 (Fig. S13b†). These values are excellent and stand out among the reported COFs.[32,33,35–41,43,44]

The Stern–Volmer constant (K_{SV}) was determined for nitroaromatic compounds based on the fluorescence

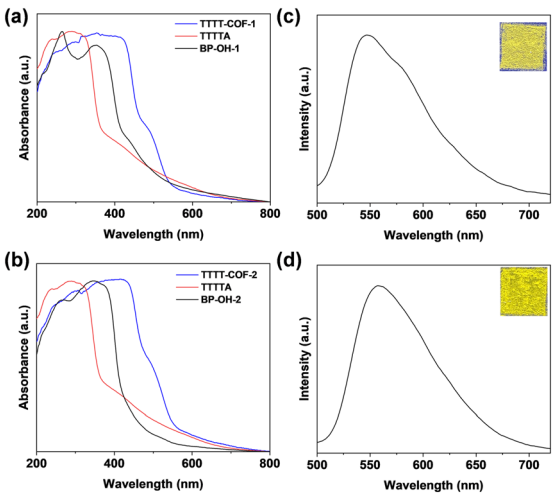

Fig. 3 Solid absorption spectra of (a) TTTT-COF-1, (b) TTTT-COF-2 and the building units. Solid fluorescence spectra of (c) TTTT-COF-1 and (d) TTTT-COF-2 (insets: photos of COFs under 365 nm).

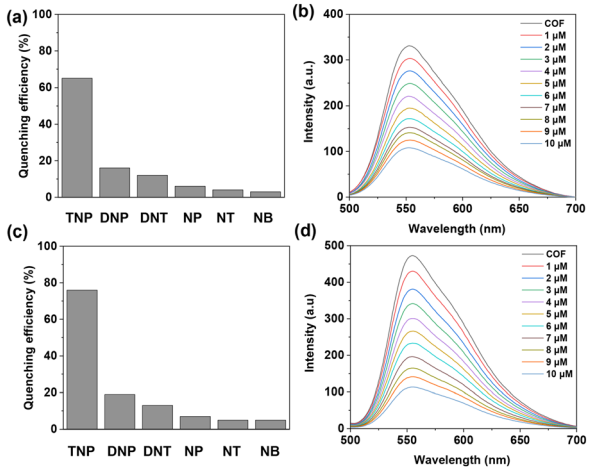

Fig. 4 Fluorescence efficiency of (a) TTTT-COF-1 and (c) TTTT-COF-2 with different nitroaromatic compounds. Fluorescence spectra of (b) TTTT-COF-1 and (d) TTTT-COF-2 with different concentrations of TNP.

Open Access Article. Published on 08 August 2024. Downloaded on 2/7/2026 4:39:54 PM. This article is licensed under a Creative Commons Attribution-NonCommercial 3.0 Unported Licence.

quenching profiles. For TTTT-COF-1, the K_{SV} was estimated to be as high as 1.26×10^5 M^{-1} for TNP (Fig. S14a†), decreasing to 2.14×10^4, 1.06×10^4, 8.46×10^3, 5.51×10^3, and 4.27×10^3 M^{-1} for DNP, DNT, NP, NT, and NB, respectively (Fig. S15a–S19a†). A similar trend was observed for TTTT-COF-2, with a high K_{SV} of 1.53×10^5 M^{-1} for TNP (Fig. S14b†). For DNP, DNT, NP, NT, and NB, the K_{SV} values decreased to 2.23×10^4, 1.46×10^4, 7.80×10^3, 4.95×10^3, and 4.73×10^3 M^{-1}, respectively (Fig. S15b–S19b†). The high K_{SV} value for TTTT-COF-2 exceeds that of the reported COFs, underscoring its excellent sensing ability.[32,33,35–41,43,44] The above interesting results can be attributed to their good porosity, mesoporous structure, and flexible channels. The high-density nitrogen and oxygen atoms within the flexible channels of TTTT-COFs can serve as hydrogen bond acceptors for nitroaromatic compounds.

Conclusions

In summary, we have successfully designed and synthesized two imine-based COFs with flexible channels through a Schiff base reaction. These COFs effectively mitigate ACQ effects by flexible channels, resulting in enhanced luminescence. Furthermore, the presence of a high density of nitrogen and oxygen atoms on these flexible walls provides binding sites for hydrogen bonding interactions, which impart sensitivity and selectivity towards nitro-explosives. This innovative strategy introduces a novel approach for developing luminescent materials for chemical sensors.

Experimental section

Synthesis of TTTT-COF-1

A 10 mL Pyrex tube was charged with TTTTA (0.1 mmol), BP-OH-1 (0.15 mmol), *o*-DCB (0.8 mL), *n*-BuOH (0.8 mL), and AcOH (0.2 mL, 6 M), and then the mixture was sonicated for 1 min and degassed through three freeze–pump–thaw cycles. The system was heated at 120 °C for 72 h. The COF was isolated by washing with tetrahydrofuran and acetone, Soxhlet extracted with tetrahydrofuran for 12 h, and dried under vacuum for 10 h to afford a yellow powder in 74% isolated yield.

Synthesis of TTTT-COF-2

A 10 mL Pyrex tube was charged with TTTTA (0.1 mmol), BP-OH-2 (0.15 mmol), *o*-DCB (0.8 mL), *n*-BuOH (0.8 mL), and AcOH (0.2 mL, 6 M), and then the mixture was sonicated for 1 min and degassed through three freeze–pump–thaw cycles. The system was heated at 120 °C for 72 h. The COF was isolated by washing with tetrahydrofuran and acetone, Soxhlet extracted with tetrahydrofuran for 12 h, and dried under vacuum for 10 h to afford a yellow powder in 71% isolated yield.

Luminescence quenching experiments

TTTT-COFs were readily dispersed in water and the obtained suspension was almost transparent. Moreover, the fluorescence spectra of the active COFs in water solutions were recorded immediately. After adding the substance, the fluorescence spectra were observed until the luminescence spectra did not show any change. Each test was repeated three times to get the average values.

Data availability

The data supporting this article have been included as part of the ESI.†

Author contributions

W. Zhao, C. Xing, Y. Zhang, J. Ren and H. Li conducted the experiments and collected the data. Y. Zhang, J. Ren and H. Li wrote the manuscript and discussed the results with all authors.

Conflicts of interest

There are no conflicts to declare.

Acknowledgements

This work was financially supported by the National Natural Science Foundation of Jilin Province (No. YDZJ202201ZYTS344).

Notes and references

1 P. J. Waller, F. Gándara and O. M. Yaghi, *Acc. Chem. Res.*, 2015, **48**, 3053–3063.
2 J. L. Segura, M. J. Mancheño and F. Zamora, *Chem. Soc. Rev.*, 2016, **45**, 5635–5671.
3 S. Yuan, X. Li, J. Zhu, G. Zhang, P. V. Puyvelde and B. V. Bruggen, *Chem. Soc. Rev.*, 2019, **48**, 2665–2681.
4 P. She, Y. Qin, X. Wang and Q. Zhang, *Adv. Mater.*, 2022, **34**, 2101175.
5 Y. Zeng, R. Zou and Y. Zhao, *Adv. Mater.*, 2016, **28**, 3032–3032.
6 J. Y. Zeng, X. S. Wang and X. Z. Zhang, *Chem. – Eur. J.*, 2020, **26**, 16568–16581.
7 Z. Meng and K. A. Mirica, *Chem. Soc. Rev.*, 2021, **50**, 13498–13558.
8 T. Skorjanc, D. Shetty and M. Valant, *ACS Sens.*, 2021, **6**, 1461–1481.
9 K. Xu and N. Huang, *Chem. Res. Chin. Univ.*, 2022, **38**, 339–349.
10 Y. Feng, G. Wang, R. Liu, X. Ye, S. Tao, M. A. Addicoat, Z. Li, Q. Jiang and D. Jiang, *Angew. Chem., Int. Ed.*, 2024, **63**, e202400009.
11 Y. Wang, X. Yang, P. Li, F. Cui, R. Wang and X. Li, *Macromol. Rapid Commun.*, 2023, **44**, 2200760.
12 Z. Li, H. Moon, S.-K. Cho, C. Li, J.-M. Seo, J.-B. Baek, H. Xu and S.-Y. Lee, *CCS Chem.*, 2023, **5**, 2567–2575.

 This journal is © The Royal Society of Chemistry 2024

Open Access Article. Published on 08 August 2024. Downloaded on 2/7/2026 4:39:54 PM. This article is licensed under a Creative Commons Attribution-NonCommercial 3.0 Unported Licence.

13 Z. Li, L. Sun, L. Zhai, K.-S. Oh, J.-M. Seo, C. Li, D. Han, J.-B. Baek and S.-Y. Lee, *Angew. Chem., Int. Ed.*, 2023, **62**, e202307459.
14 L. Zhai, Y. Yao, B. Ma, M. M. Hasan, Y. Han, L. Mi, Y. Nagao and Z. Li, *Macromol. Rapid Commun.*, 2022, **43**, 2100590.
15 Y. Wang, Y. Zhao and Z. Li, *Macromol. Rapid Commun.*, 2022, **43**, 2200108.
16 (*a*) C. Yang, Z. Zhang, J. Li, Y. Hou, Q. Zhang, Z. Li, H. Yue and X. Liu, *Green Chem.*, 2024, **26**, 2605–2612; (*b*) S. Zhu, Z. Zhang, Z. Li and X. Liu, *Mater. Chem. Front.*, 2024, **8**, 1513–1535.
17 R. Nie, W. Chu, Z. Li, H. Li, S. Chen, Y. Chen, Z. Zhang, X. Liu, W. Guo and S. I. Seok, *Adv. Energy Mater.*, 2022, **12**, 2200480.
18 A. F. M. EL-Mahdy, M.-Y. Lai and S.-W. Kuo, *J. Mater. Chem. C*, 2020, **8**, 9520–9528.
19 W. Ma, S. Jiang, W. Zhang, B. Xu and W. Tian, *Macromol. Rapid Commun.*, 2020, **41**, 2000003.
20 C. Krishnaraj, A. M. Kaczmarek, H. S. Jena, K. Leus, N. Chaoui, J. Schmidt, R. V. Deun and P. V. D. Voort, *ACS Appl. Mater. Interfaces*, 2019, **11**, 27343–27352.
21 Y. Lu, Y. Liang, Y. Zhao, M. Xia, X. Liu, T. Shen, L. Feng, N. Yuan and Q. Chen, *ACS Appl. Mater. Interfaces*, 2021, **13**, 1644–1650.
22 W. Gong, Y. Dong, C. Liu, H. Shi, M. Yin, W. Li, Q. Song and C. Zhang, *Dyes Pigm.*, 2022, **204**, 110464.
23 H. Q. Yin, F. Yin and X. B. Yin, *Chem. Sci.*, 2019, **10**, 11103–11109.
24 J. Wan, W. Shi, Y. Li, Y. Yu, X. Wu, Z. Li, S. Y. Lee and K. H. Lee, *Macromol. Rapid Commun.*, 2022, **43**, 2200393.
25 L. Yuan, J. Zhu, S. Wu and C. Chi, *Chem. Commun.*, 2022, **58**, 1302–1305.
26 H. Zhu, T. M. Geng and K. B. Tang, *Microporous Mesoporous Mater.*, 2022, **343**, 112165.
27 G. Das, B. P. Biswal, S. Kandambeth, V. Venkatesh, G. Kaur, M. Addicoat, T. Heine, S. Vermab and R. Banerjee, *Chem. Sci.*, 2015, **6**, 3931–3939.
28 Z. Li, Y. Zhang, H. Xia, Y. Mu and X. Liu, *Chem. Commun.*, 2016, **52**, 6613–6616.
29 S. Y. Ding, M. Dong, Y. W. Wang, Y. T. Chen, H. Z. Wang, C. Y. Su and W. Wang, *J. Am. Chem. Soc.*, 2016, **138**, 3031–3037.
30 W. Gong, C. Liu, H. Shi, M. Yin, W. Li, Q. Song, Y. Dong and C. Zhang, *J. Mater. Chem. C*, 2022, **10**, 3553–3559.
31 X. Li, Q. Gao, J. Wang, Y. Chen, Z. H. Chen, H. S. Xu, W. Tang, K. Leng, G. H. Ning, J. Wu, Q. H. Xu, S. Y. Quek, Y. Lu and K. P. Loh, *Nat. Commun.*, 2018, **9**, 2335.
32 M. Yang, H. Hanayama, L. Fang, M. A. Addicoat, Y. Guo, R. Graf, K. Harano, J. Kikkawa, E. Jin, A. Narita and K. Müllen, *J. Am. Chem. Soc.*, 2023, **145**, 14417–14426.
33 Y. Zhang, Y. Zhao, C. Zhang, X. Luo and X. Liu, *CrystEngComm*, 2022, **24**, 4496–4499.
34 C. Gong, C. Yan, J. Liu, J. Li, J. Fu, C. Chen, Y. Huang, G. Yuan and Y. Peng, *TrAC, Trends Anal. Chem.*, 2024, **173**, 117625.
35 Z. Li, K. Geng, T. He, K. T. Tan, N. Huang, Q. Jiang, Y. Nagao and D. Jiang, *Angew. Chem., Int. Ed.*, 2021, **60**, 19419–19427.
36 G. Lin, H. Ding, D. Yuan, B. Wang and C. Wang, *J. Am. Chem. Soc.*, 2016, **138**, 3302–3305.
37 X. Liu, Y. Han, G. Wang, Y. Wang, J. Chen, Y. Shu, J. H. Wang and H. Qiu, *ACS Appl. Nano Mater.*, 2022, **5**, 6422–6429.
38 C. Zhang, S. Zhang, Y. Yan, F. Xia, A. Huang and Y. Xian, *ACS Appl. Mater. Interfaces*, 2017, **9**, 13415–13421.
39 M. W. Zhu, S. Q. Xu, X. Z. Wang, Y. Chen, L. Dai and X. Zhao, *Chem. Commun.*, 2018, **54**, 2308–2311.
40 S. Dalapati, S. Jin, J. Gao, Y. Xu, A. Nagai and D. Jiang, *J. Am. Chem. Soc.*, 2013, **135**, 17310–17313.
41 Q. Gao, X. Li, G. H. Ning, K. Leng, B. Tian, C. Liu, W. Tang, H. S. Xu and K. P. Loh, *Chem. Commun.*, 2018, **54**, 2349–2352.
42 J. H. Song and D. W. Kang, *Coord. Chem. Rev.*, 2023, **492**, 215279.
43 J. Q. Chen, Q. Q. Zheng, S. J. Xiao, L. Zhang, R. P. Liang, G. Ouyang and J. D. Qiu, *Anal. Chem.*, 2022, **94**, 2517–2526.
44 Y. Han, Y. Chen, J. Feng, J. Liu, S. Ma and X. Chen, *Anal. Chem.*, 2017, **89**, 3001–3008.